Materials Science-Poland, 41(1), 2023, pp. 110-123
http://www.materialsscience.pwr.wroc.pl/
DOI: 10.2478/msp-2023-0008

sciendo

Comparison of the performance properties of commercially produced roller cone bit coatings

Sylwia Koczkodaj[1,*], Jaroslaw Mizera[1], Dorota Moszczynska[1], Joanna Zdunek[1], Magdalena Plocinska[1], Jacek Szpyrka[2], Marek Burkot[2], Mateusz Szpak[2]

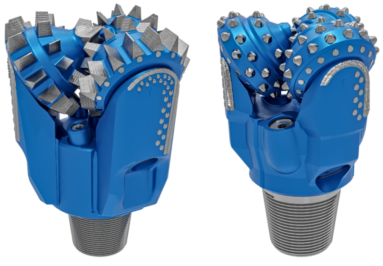
[1]Faculty of Materials Science and Engineering, Warsaw University of Technology, 141 Woloska St, 02-507 Warsaw, Poland
[2]Glinik Drilling Tools, 1 Michalusa St, 38-320 Gorlice, Poland

This paper studies the material aspects of roller cone bits with milled teeth. The research concerns the properties of commercial product overlays provided by the company Glinik Drilling Tools. The analyzed coatings were produced according to the company's procedures using two surfacing methods: gas welding and plasma transferred arc (PTA) welding. Metallographic observations and chemical composition analyses were carried out. The evaluation criteria in the context of the surfacing application were mechanical properties: hardness, impact strength, and abrasion resistance. The overlays produced by gas welding were characterized by lower hardness, impact strength, and abrasion resistance. The study showed that it differed from the deposit made by the PTA method in the matrix material and in the average size of the tungsten carbides. The dissolution of primary carbides and formation of secondary carbides such as Fe_3C and $Ni_{17}W_3$ were found to occur in both surfacing types. This contributes to the increased brittleness of the matrix and reduced wear resistance of the materials.

Keywords: *roller cone bit, carbide coating, mechanical properties, gas welding, plasma transferred arc welding*

1. Introduction

Roller cone bits, second only to polycrystalline diamond compact (PCD) bits, are currently the primary tool used in the drilling industry. They are made of three interconnected segments, named lugs or arms, which constitute the bit body. At the end of each of them is a rotating cone on a bearing journal. Due to the types of bearings, roller cone bits are divided into those with roller or friction bearings, sealed or unsealed. Each cone has a few rows of cutting elements (milled teeth or TC inserts, see Figure 1) designed to drill the rock. The degrees of hardness of cutting structures on bits are designed according to the International Association of Drilling Contractors (IADC) code for different formations. Bits with teeth work together to drill the rock formations and, at the same time, clean each other of the spoil. Inside the segments, channels end with nozzles, supplying the drilling fluid. The central nozzle is designed to bring the drilling fluid to the bottom of the hole, and the nozzles around the perimeter ensure the cleaning and cooling of the bearings. Due to the flushing system, the following types can be identified: center (1 nozzle), 3-jet (3 nozzles), and multi-jet flushing system (4 nozzles) [1, 2]. In this article, the authors focus on the material aspects of roller cone bites with milled teeth.



(A) (B)

Fig. 1. Types of roller cone bits: (a) milled-tooth bits, (b) insert-tooth bits – Glinik Drilling Tools product catalog [2]

The roller cone bits excavate the rock formation in two ways. Strong bit loading forces press the teethes or inserts into the rock and crush it.

* E-mail: sylwia.koczkodaj.dokt@pw.edu.pl

© Sylwia Koczkodaj et al. 2023. This is an open access article distributed under the Creative Commons Attribution-NonCommercial-NoDerivatives 4.0 License. (http://creativecommons.org/licenses/by-nc-nd/4.0/)

Rotation speed and torque drive the bit around the vertical axis, which drives the cones to rotate around their axis (slightly angled to the axis of bit rotation). This causes the cutting elements to exert a lateral force on the rock and shear its fragments [1, 3, 4].

The effective life of a roller cone bit is affected by the following factors: the construction parameters of bits (e.g., the shape and size of the teeth and their arrangement), type of drilling rocks (geomechanical properties), drilling parameters (e.g., weight on bit (WOB), rotary per minute (RPM), total bit revolutions (kRev), flow rate of mud), and properties of the materials from which its elements are made [5–7]. Bearing and teeth failures are the most common causes of shortened drill bit life [8, 9]. Many authors have examined the wear of roller cone bit teeth [3, 5–10]. Larsen-Basse [10] concluded that the main mechanisms are impact fracturing, mechanical fatigue due to overloads, abrasion wear, and thermal fatigue. Further research shows that the primary type of abrasion wear in a soft rock formation is caused by ploughing and, in hard formation, by micro-ploughing and microcutting [5]. During drilling, the bit material heats up in contact with the rock and then cools down with the drilling fluid contact. As a result of the differences in thermal properties (coefficients of expansion) of the carbide coating and the tooth core, microcracks can be formed, which results in the penetration of the dispersed medium, which contains erosive particles, and further degradation of the material. However, this wear mechanism and mechanical fatigue due to overloads can be minimized by adequately selecting the drilling regime and drilling fluid flow [3, 7].

As mentioned above, the material's properties are one factor that influences the effective life of a roller cone. The companies manufacturing them do not make the materials used to produce the bits and their chemical compositions public. On the basis of the study of damaged drills, however, it can be concluded that the teeth of the bits consist of three layers: an outer hard-facing layer containing tungsten carbides in a steel or nickel matrix, a second layer of high-carbon martensitic steel, and a third layer (tooth core) of low-carbon martensitic steel [5, 7, 11]. Due to the specificity of the drill work, it is essential that the bit material is characterized by both wear resistance and chipping resistance. During the production of the material, it is crucial to find the trade-off between these two parameters. Many metal matrix composites (MMC) were tested. The typical composite material consists of hard tungsten carbides providing wear resistance and a soft matrix (usually Fe-, Ni-, and Co-based alloy) that improves ductility and impact strength. It is characterized by excellent chemical and mechanical properties such as hardness, resistance to cracking, and abrasive wear. The low price and high performance of Fe-based, self-fluxing alloy result in their being widely used [12]. Currently in the research spotlight are WC-Ni systems, which seem to exhibit the best performance in cutting tool production. A typical hardfacing nickel matrix contains silicon, boron, and sometimes chromium. The alloying elements are added to lower the melting point and reduce the dissolution of the strengthening phase but also to reinforce the matrix. The creation of nickel borides and nickel silicides improves wear resistance. The currently most commonly used strengthening phase is cemented carbide composed of tungsten carbide and cobalt (WC-Co). Cobalt increases the wettability of the tungsten carbide particles, which improves their binding. Among all hard phases in carbides, the most significant is hexagonal tungsten monocarbid (WC), but tungsten dicarbid (W_2C) is also used. Several types of tungsten carbides, depending on the manufacturing technique, the type of carbide, the WC/W_2C ratio, and resulting properties can be indicated, e.g., fused and crushed tungsten ratio (FTC), spherical tungsten carbides (SCC), macrocrystalline tungsten carbide (MTC) [13–19].

The protective layer is applied not only to protect the cutting structure but also to protect the diameter of the bit. For that, the teeth in the last row and the back of the arm are additionally strengthened. In addition to the surfacing, carbide inserts are also used as reinforcement. Both types of reinforcement are shown in Figure 2. Although there is much data in the literature on manufacturing layers using modern methods such as laser deposition

commercially, gas deposition is still predominantly used. Recently, plasma deposition has been gaining attention, mainly due to the reproducibility of the process and the possibility of automation. However, there are still problems with the selection of parameters in the case of small tool diameters and complex tool geometries. The impact of the production processes on the microstructure of the layer and the resulting properties is significant because it directly affects the quality of the bit and its service life.

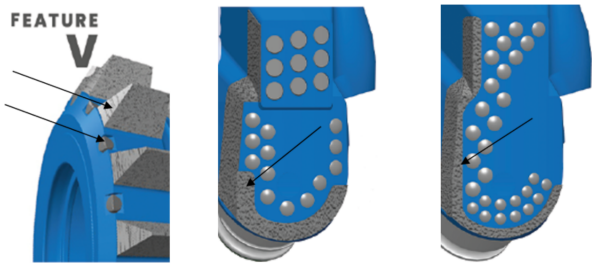


Fig. 2. Different types of teeth and arms reinforcements [2]. The arrows mark the locations of the overlays

The motivation to undertake this research was the lack of studies on the properties of overlays on commercial products applied to cones by various methods. A wide range of materials for drilling tools was tested under optimal laboratory conditions [16, 18–21]. There is little updated research on the material aspects of roller cone bits, which has mainly focused on failure analysis or causes of wear [5, 7, 11, 22]. The research aim was to compare the microstructure and mechanical properties of overlays made by gas weld surfacing and plasma transferred arc (PTA) welding to evaluate their application on roller cone bits. The assessment criteria were hardness, impact strength, and abrasion resistance.

2. Material and methods

2.1. Material

The tests were carried out on samples provided by Glinik Drilling Tools. The rectangular samples (Figure 3) were prepared using commercial materials by gas welding and plasma transferred arc (PTA) welding methods. Depending on the characteristics of the method, rod and powder were used to produce the overlay, respectively. The exact chemical composition and manufacturing parameters are company "know-how" and therefore proprietary. All samples were heat treated after welding, which included carburizing, hardening, and tempering. The exact heat treatment parameters are proprietary information. On the delivered samples, metallographic sections were made and subjected to microstructural analysis. Mechanical properties were evaluated.



(A)



(B)

Fig. 3. The samples submitted for testing by Glinik Drilling Tool: (a) gas welding; (b) plasma transferred arc welding

2.2. Methods

2.2.1. Light microscopy

Microscopic observations of the samples were carried out using Nikon Epiphot and Kayence VHX200 light microscopes. The samples were observed without and with etching with Murakami's reagent. The study aimed to observe the obtained layer and analyze the material's structure and defects.

2.2.2. Stereology

Photos of the analyzed layers were taken using a Keyence VHX600 microscope, which was then binarized using the Met-Ilo program to determine

the volume fraction of WC. The images obtained were analyzed in the Micrometer program, which allows for determining the volume fraction and particle size distribution.

2.2.3. Scanning electron microscopy

Microscopic observations were made using the scanning electron microscope SU 8000 by Hitachi. Observations were made in the magnification range from 30 to 50000. The accelerating voltage of the electrons was set at 5–30 kV. The observations were made using the secondary electron (SE) and back-scattered electron (BSE) detector. Microanalysis of the chemical composition of the samples, including qualitative and quantitative analysis, was determined using an energy-dispersive spectrometer (EDS) by ThermoFisher.

2.2.4. X-ray diffraction (XRD)

The phase composition was determined using a Bruker D8 Discover x-ray diffractometer working in a point beam geometry with a 1.5-mm collimator, using non-monochromatic CoKα radiation. An iron filter was used to cut the CoKβ line. The measurement conditions were as follows: the 2θ range was 20°–130°, step 0.05, and sampling time 3 s per step using the position-sensitive detector (PSD) Vantec 1 strip detector. The records were compared to patterns from the ICDD PDF-2 database using the DiffracEva program (Bruker).

2.2.5. Microhardness test

Microhardness tests using the Vickers method were performed on the Falkon500 device, according to the PN-EN ISO 6507-1 standard "Microhardness tests." Measurements were made in the overlay area and the base material.

2.2.6. Impact test

The impact test was carried out on a Charpy SUNPOC JB300B impact hammer with an initial energy of 300 J, following the requirements of PN-EN ISO 148-1:2010. The tests were performed at room temperature on five specimens from each series. Samples with a U-shaped notch on the opposite side of the surfacing were used. Because the specimens were not identical, and the surfacing was only a tiny part of the specimen cross-section, these results cannot be considered conclusive. Still, they can be used for comparison purposes between the two series.

2.2.7. Abrasion test

Following ASTM G 6-00, Procedure A, Abrasion tests were conducted under laboratory conditions. For each combination, tests were carried out in five repetitions. In addition, tests were performed on three samples of Hardox 450 steel, which was the reference material. Each sample was ground to obtain flatness and straightness of the surface. The abrasive wheel made 6,000 revolutions during the test, and the abrasive flow rate (A. F. S. testing Stand 50-70 sand) was 335 g/min. To determine weight loss, samples were weighed to the accuracy of 0.0001 g before and after the tests. The average density of the overlays was determined using a WAX 60/220 RADWAG laboratory balance based on measurements of samples weighed in air and demineralized water. Volumetric weight loss (mm^3) was calculated as the weight loss ratio to density. The results were compared to the abrasive wear resistance of Hardrox 450 steel by determining the relative abrasive wear resistance of the metal-mineral type of surfaced layers.

3. Results and discussion

3.1. Microstructural analyses

The cross-section of the overlay made by gas welding is shown in Figure 4. The overlay thickness was from 22 to 25 mm. The consistent and uniform microstructure of the layer proves the good weldability of the material. Microscopic observations did not reveal the presence of discontinuities such as pores or cracks throughout the overlay. However, the dissolution of tungsten carbide particles is observed in the bottom part of the overlay, which is clearly visible during mapping analyses (Figure 5). The basic material used by the Glinik Drilling Tools company is a gas surfacing rod, which, as the manufacturer declares, consists of a steel tube filled with a mixture of WC and Si-Mn alloy. This information is consistent with the



Fig. 4. Cross-section of the coating made by the gas weld surfacing

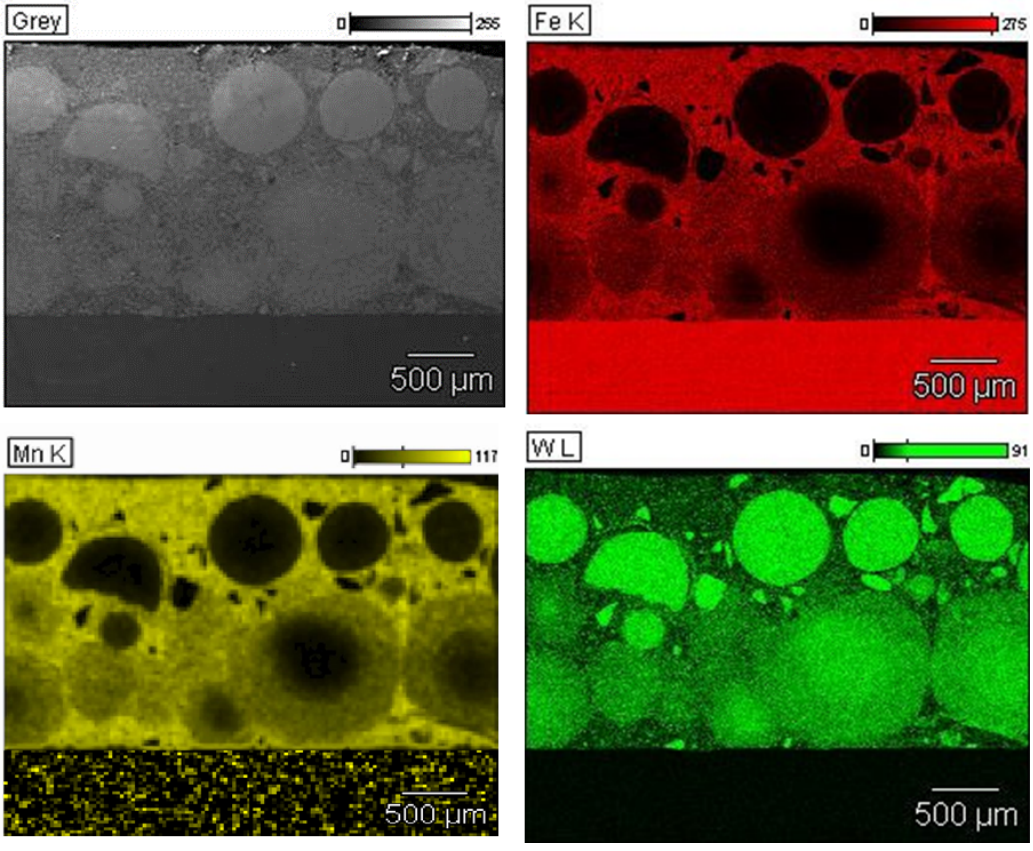


Fig. 5. Mapping of key elements of the gas weld surfacing layer

chemical composition analyses performed.

Spherical and polyhedral particles are visible inside, with a 50.7% and 4.7% volume fraction, respectively. The diameter of the spherical particles was in the range of 400 to 600 µm. The different microstructures of particles are demonstrated in Figure 6. The spherical particles are characterized by typical features of cermet with well-bonded prismatic WC grains and Co matrix [18, 19].

EDS analysis (Figure 7, Table 1) was used to characterize the particles observed. It showed that both contain predominant amounts of tungsten, iron, and carbon. Polyhedral and spherical particles differ in that the first also contains nickel and is richer in iron (spots 1 and 3), and in the second (spots 2 and 4), cobalt is also detected.

The cross-section of the overlay made by PTA is shown in Figure 8. The PTA overlay's thickness was lower than that made by gas welding and amounted to 15–17 mm. Similarly, the coating was well bonded with the steel base and uniform without defects like microcracks or pores. The main

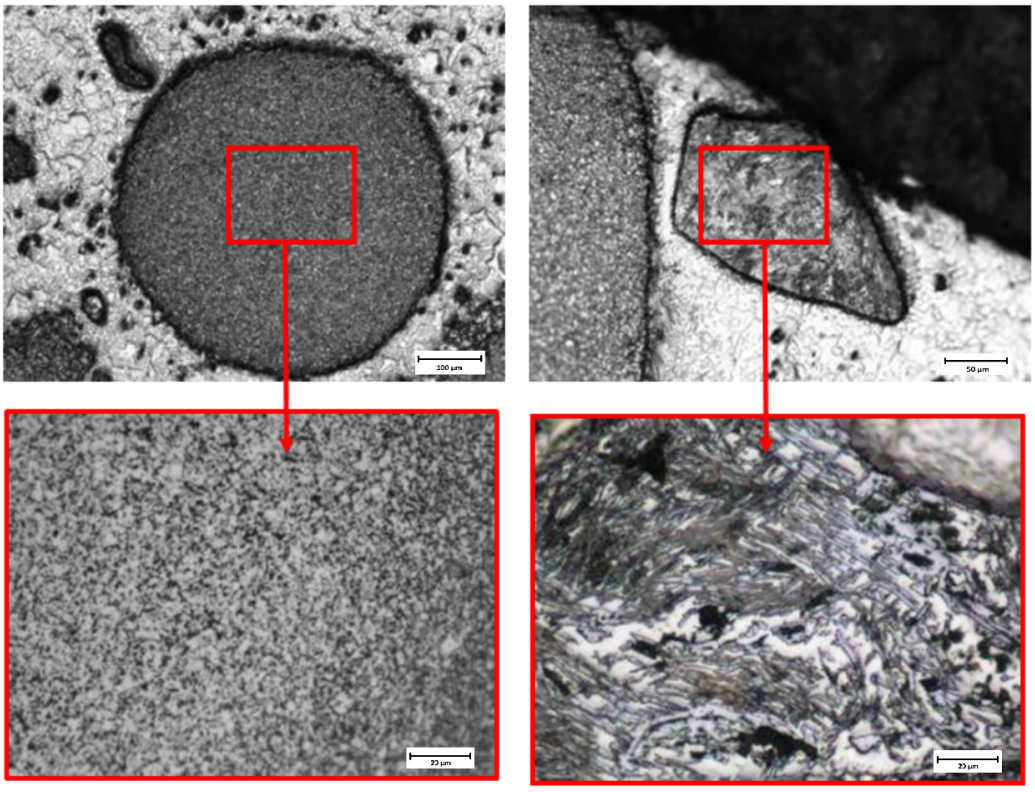


Fig. 6. Spherical and polyhedral particles in the gas weld surfacing

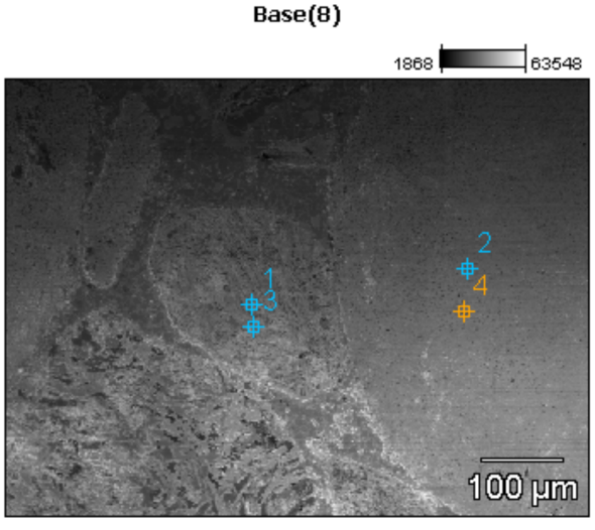


Fig. 7. SEM micrographs of overlay made by gas welding surface with EDS spot analysis

particles had spherical shapes; however, their concentration was lower in some parts of the overlay. Comparably to the previous overlay, the volume

Table 1. EDS spot analysis of the areas in Figure 7 (weight %)

	C-K	*Fe-K*	*Ni-K*	*Co-L*	*W-M*
Base(8)_pt1	2.2	2.6	0.8		94.4
Base(8)_pt2	3.5	1.6		0.2	94.7
Base(8)_pt3	1.8	3.5	0.3		94.4
Base(8)_pt4	2.9	2.2		0.6	94.3

fraction of the strengthening phase was 55%. The particles were finer, however, and their diameter was about 120 µm. The distribution of primary elements in the whole was similar to the gas-welded overlay (Figure 9). According to the company, the powder used to make overlay by PTA methods contains WC and nickel alloy as a matrix, which is in line with mapping and EDS results (Figure 9). The enrichment of iron observed in the fusion zone may be caused by the diffusion of the element during the surfacing process; similar results were observed by Li et al. [23].

Microstructure analysis using a scanning elec-

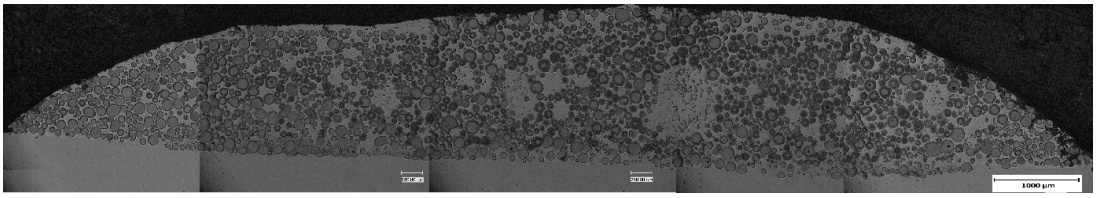


Fig. 8. Cross-section of the coating made by the PTA weld surfacing

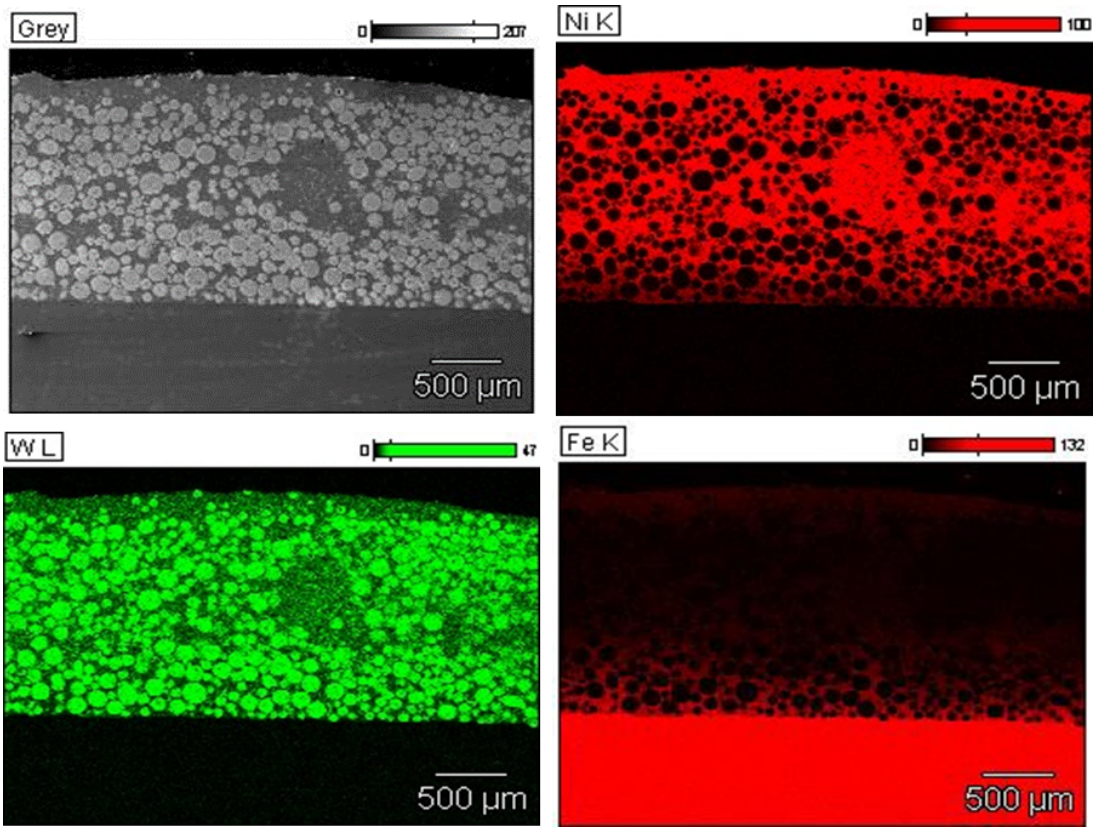


Fig. 9. Mapping of key elements of the PTA weld surfacing layer

Table 2. EDS spot analysis of the areas in Figure 11 (weight %)

	C-K	Cr-K	Fe-K	Ni-K	W-L
Base(49)pt1	6.6	0.3	1.5	18.4	73.2
Base(49)_pt2	3.6	0.2	0.9	13.8	81.6
Base(49)_pt3	5.9	0.2	0.7	8.8	84.5
Base(49)_pt4	4.3	0.2	0.9	12.6	81.9
Base(49)_pt5	3.8	0.3	1.1	14.9	79.9
Base(49)_pt6	3.7	0.2	0.9	16.0	79.2
Base(49)_pt7	5.4		0.1		94.3
Base(49)_pt8	5.4		0.2		88.9

tron microscope revealed two morphological zones in the padding weld, differing microstructure elements caused by the coating application process, and the parameters used (Figure 10). The first zone is the fusion zone of the surfacing with the base material. The surfacing adheres tightly to the base material. Visible deformations can be caused by the impact of hard particles on the substrate material during the process. In the matrix, the eutectics are clearly visible. In zone two, carbides are seen in the dendrites' nickel matrix. In each zone, secondary carbides are visible, mainly formed around the

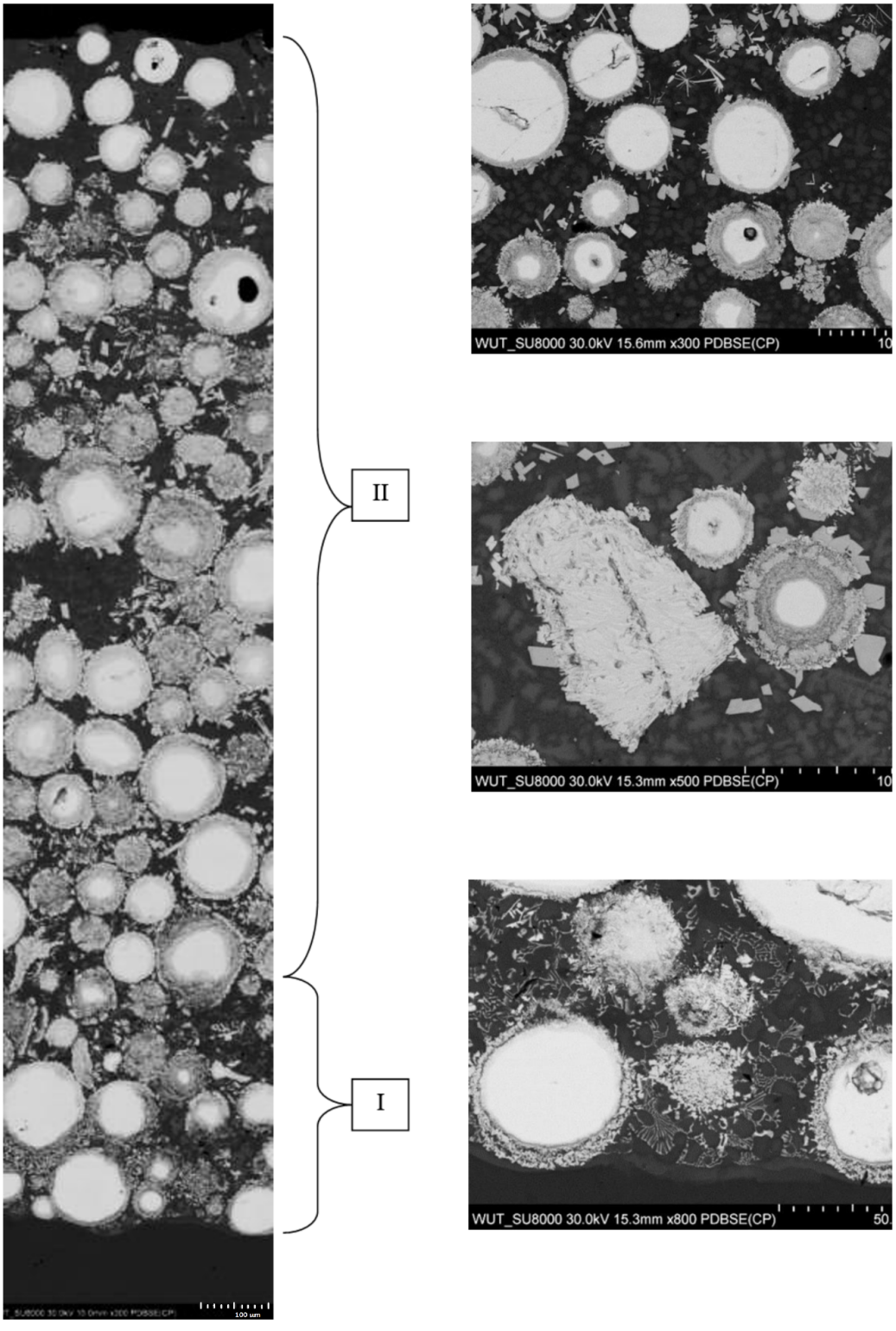


Fig. 10. The microstructure of the coating is made by PTA weld surfacing with the distinction of three zones occurring in the layer

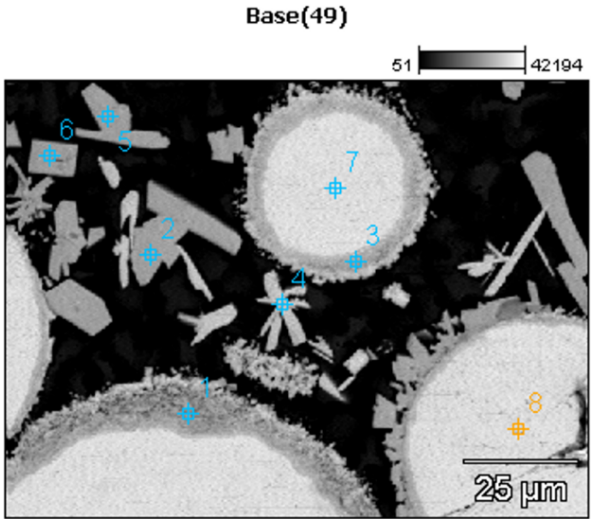


Fig. 11. SEM micrographs of overlay made by PTA surface with EDS spot analysis

primary ones. Other authors observed similar microstructures in a study of materials strengthened with WC particles [24–26]. The dendritic structures with motile, floral, star-shaped, and block-shaped carbides were formed by the melting of tungsten carbide particles during the surfacing process. The formation or not of dendritic structures in the matrix depended on the parameters of the layering process [23]. A detailed study on the microstructure analysis of Ni-WC surfaced layers using transmission electron microscopy (TEM) was carried out by Liyanage and coauthors [26]. A Ni-base matrix composed of a eutectic mixture of dendrites and interdendritic, identified as γ-Ni dendrite eutectic and γ-Ni+Ni_3B eutectic, respectively.

EDS analyses of blocky-shaped structures (Figure 11, Table 2) also confirmed the partial dissolution of the tungsten carbides and formation of transition phases between the matrix and the reinforcing particle, in agreement with the literature [16, 18, 20, 26]. Inside the spherical particles, only tungsten and carbide were detected. The η carbides also consist of various chromium, iron, and nickel quantities. Figures 12 and 13 show the phase composition of the samples made using gas and plasma methods. In the first one, only WC tungsten carbide occurs; in the second, two types occur: WC and W_2C. Both overlays contain nickel tungsten of the formula $Ni_{17}W_3$. Gas-welded overlay also has phases, such as iron, carbon, and iron tungsten carbide (Fe_3W_3C) and overlay composed of PTA nickel and carbon. There are also differences regarding the peaks' half-width and intensity. The broadening of the peaks from tungsten carbide in the PTA-generated overlay may indicate the state of dispersion of this phase and the presence of residual stresses in the coating. The differences in peak intensities from the same phases in different coatings may be due to the different textures of these phases caused by different manufacturing methods. The available data in the literature show that complex secondary carbides form at the interface between the primary carbide (WC) and the matrix, formed from a solution supersaturated with carbon and tungsten. The higher diffusion coefficient of carbon in the matrix than in the carbide-forming metal contributes to faster diffusion out of the carbide, allowing the creation of some forms of mixed carbides [27]. The tungsten carbide is sensitive to high temperatures despite the high melting points of 2870°C and 2730°C for WC and W_2C, respectively. The self-fluxed nickel alloys, with melting temperatures between 1000 and 1100°C, are used for hardfacing to avoid degradation of tungsten carbides. Adding boron and silicon is intended to lower the melting point and reduce the heat impact. The addition of chromium to nickel alloys is questionable. On the one s-hand, its presence increases the hardness of the matrix, improves corrosion resistance, and prevents porosity through carbon capture. On the other hand, it facilitates carbide dissolution, increasing matrix brittleness and susceptibility to cracking. For this reason, nickel alloys with chromium are recommended in processes with less heat input and a slow solidification rate, like manual gas welding but not PTA. The dissolution of carbide is also influenced by its type and shape. Macro crystalline tungsten carbide is more stable and less prone to dissolve than the eutectic WC/W_2C carbides. Irregularly shaped carbides tend to dissolve faster because they tend to heat up locally. Additionally, fine carbides are more prone to dissolving than coarse ones [18, 20, 28, 29]. WC is a line compound with insignificant deviation from stoichiometric compo-

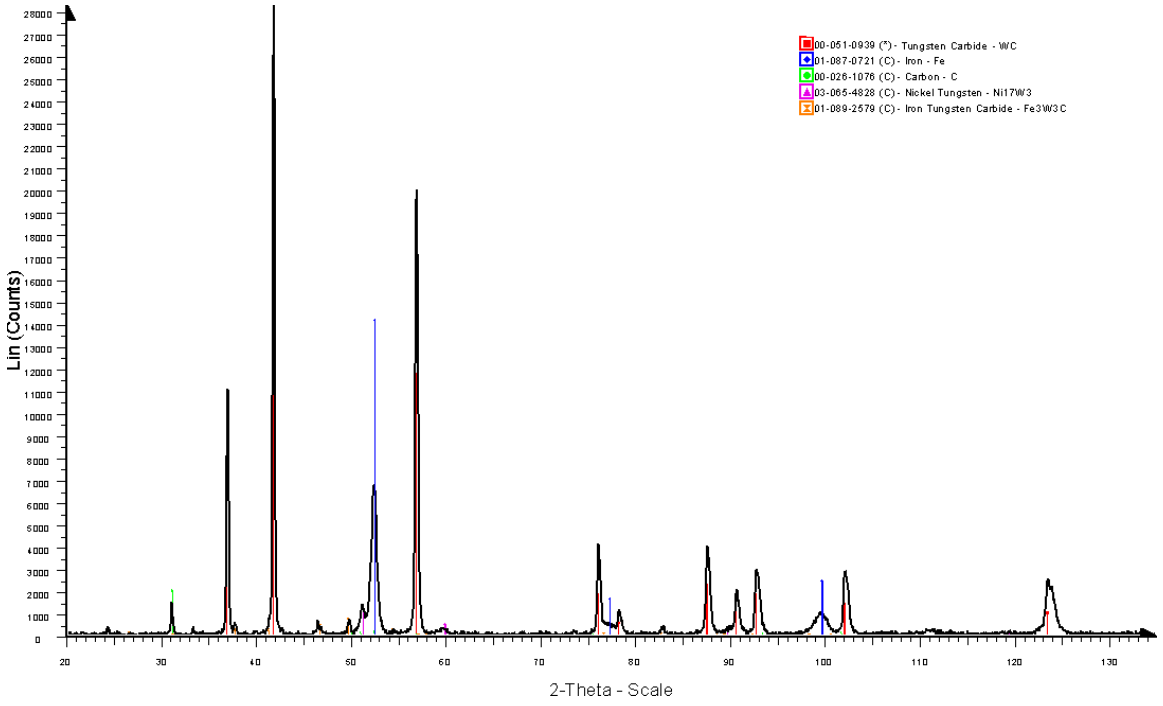


Fig. 12. Results of XRD analyses on sample cross-section made by gas weld surfacing

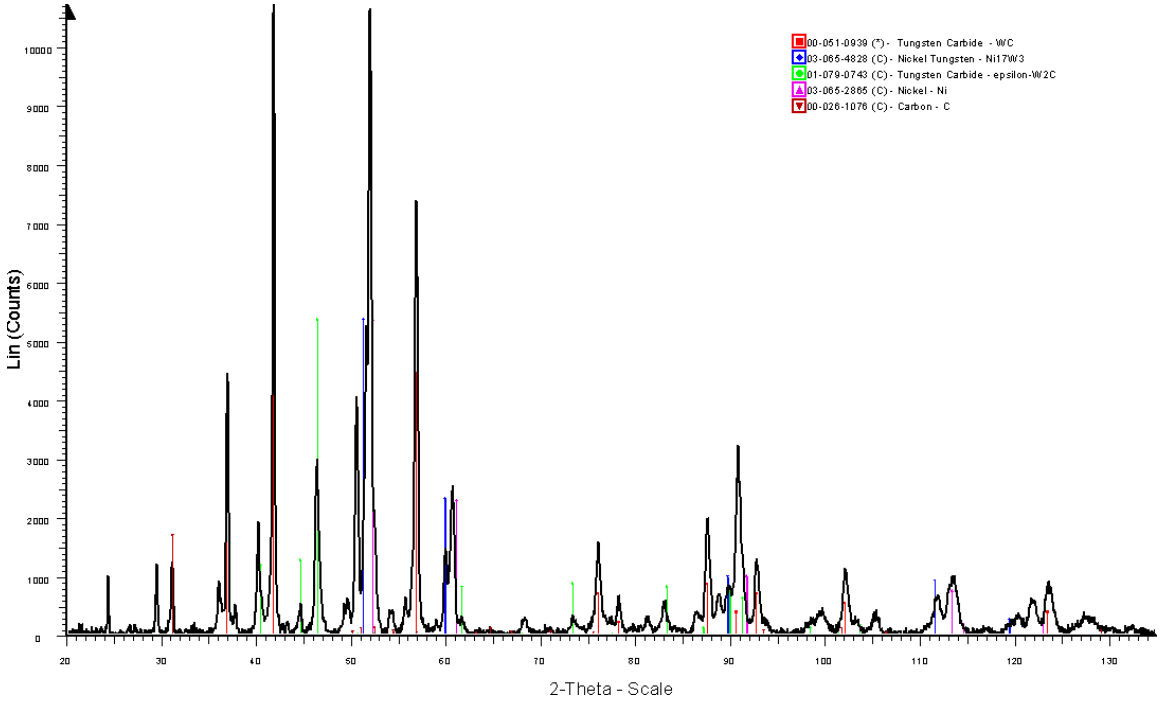


Fig. 13. Results of XRD analyses on sample cross-section made by PTA

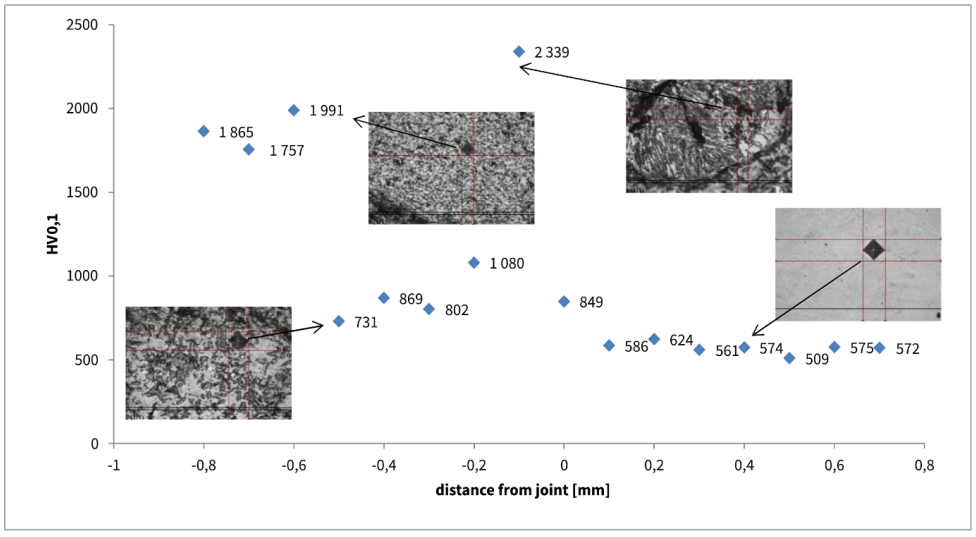


Fig. 14. Microhardness distribution on sample cross-section made by gas weld surfacing (0mm-joint)

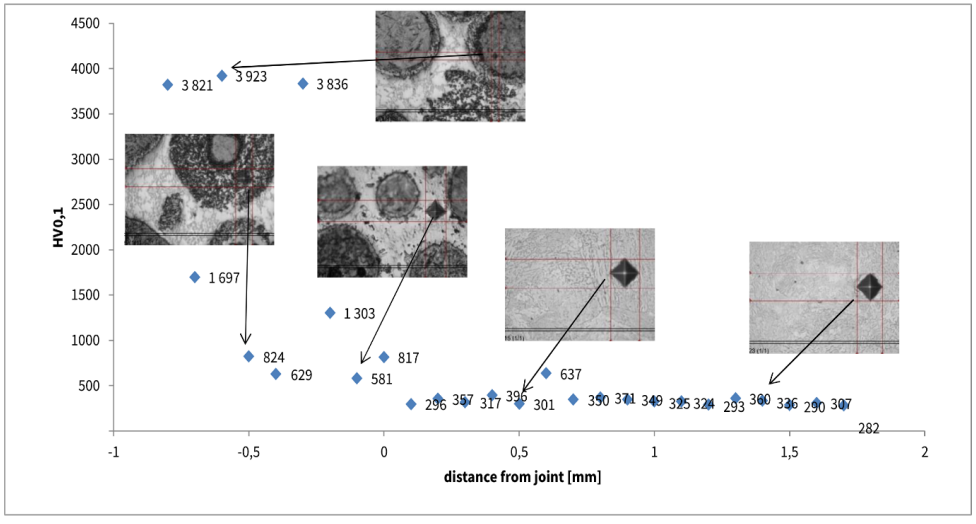


Fig. 15. Microhardness distribution on sample cross-section made by PTA weld surfacing (0mm-joint)

sition. The dissolved WC particles will participate in two ways depending on the carbon concentration in the base alloy. If it is high, smaller WC particles can be formed. In the opposite situation, W_2C and η phase complex carbides can occur. W_2C has three types—α-W_2C, β-W_2C, and γ-W_2C—which can undergo polymorphic transformation at high temperature (2000–2776°C). η phase complex carbides are formed as a result of dissolved tungsten and carbon reacting with the matrix elements, like nickel or chromium. They exist in wide stoichiometries, but the most common are M_6C and $M_{12}C$. Carbides like M_7C_3 and $M_{23}C_6$ occur less frequently because they are better stabilized by the Cr content in the alloy [23, 26, 30]. Hamar-Thibault et al. [31] have also identified the occurrence of more complex forms with the chemical formula $(NiSi)_A(CrW)_B$. This information is consistent with the identification of phase $Ni_{17}W_3$ present in both tested surfacings (Figure 12). Either W_2C and η phase carbides, like those present in the analyzed samples Fe_3W_3C, are brittle and have poor chemical and wear resistance compared to the WC.

Table 3. HV 0.1 microhardness measurements

	Basis (steel)	Matrix	Strengthening phase
Gas Welding			
average	567.0	1028.2	1699.8
SD	23.6	60.6	245.4
PTA			
average	352.6	714.2	3707.6
SD	26.7	162.4	237.2

3.2. Mechanical properties

The results of the microhardness tests are shown in Table 3 and Figures 14 and 15. The impressions were made in both the base and the surfacing, taking 0 points as the joint. In the sample made by gas welding, both the base and matrix of the surfacing exhibited higher hardness compared to the sample made using the PTA method. An inverse correlation was observed for the strengthening phase. In both cases, the hardness of the coating matrix was about twice that of the steel base material. Changes in matrix microhardness are related to the dissolution of the tungsten carbides and the formation of secondary carbides during surfacing. Similar results were observed by Maroli and Dizdar [20] and Czupryński [21]. The microhardness tests showed that structures identified as secondary carbides show lower hardness than tungsten carbides, but higher hardness than the matrix. It confirms the data in the literature about the hardness of secondary eta carbides [18]. The tungsten carbides also showed a high range of variability. Garcia-Ayala et al. [19] pointed out that the hardness, and consequently the toughness of tungsten carbides, is a function of the average WC grain size and content of Co. The finer grains and lower Co content increase hardness. The highest hardness shows carbides with ultrafine grains amounted to 0.2–0.5 μm. On this basis, it can be concluded that the strengthening phase used in plasma surfacing has a finer structure and/or lower Co content. Yang et al. [32] pointed out that an increase in microhardness positively correlates with the material's wear resistance and negatively with the resistance to brittle fracture.

The impact test results are shown in Figure 16. It is worth noting that these results can only be used

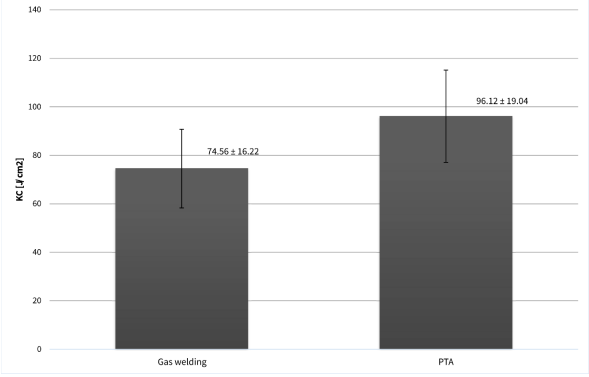


Fig. 16. Comparison of the impact test results of samples made by Gas welding and PTA

to compare series (explanation in section 2.2.6. *Impact test*). Fracture toughness mainly depends on the bonding phase type and the absence of destructive brittle phases like η carbides, which can lead to the initiation and propagation of the cracks [33]. The samples made by the PTA method with the Ni matrix showed higher resistance to dynamic loads. However, it can be speculated that the presence of secondary carbides reduces the strength of the fracture toughness.

The comparison of relative abrasion resistance of the analysis series is shown in Figure 17. Overlay made by the PTA method characterized two times better abrasive wear resistance than series produced by gas welding. The abrasive wear of welding overlays depends on several structural factors, for example, the tungsten carbides' amount, shape, and distribution. However, there is a maximum content for the reinforcement phase (depending on the welding methods and matrix phase), above which there are problems with aggregation and bonding with the matrix. There is also a significant influence on the degree of dissolution of

the WC, which depends on the matrix's chemical composition and the welding process parameters [12, 16, 20, 33, 34]. The higher wear resistance correlates with higher WC content and finer particles. As with impact strength, the presence of the eta phase contributes to the deterioration of wear resistance.

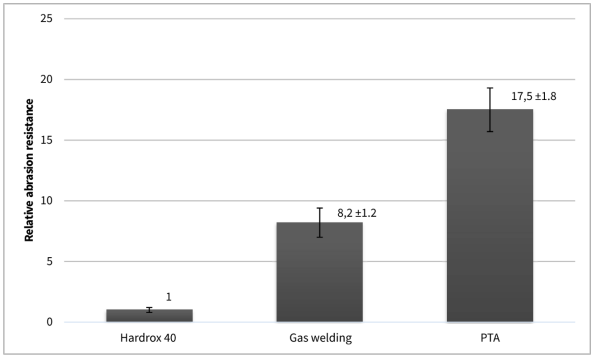


Fig. 17. Comparison of the relative abrasion resistance of samples made by gas welding and PTA

4. Conclusions

In summary, the plasma-generated surfacing was characterized by a more homogeneous structure and higher fragmentation of the reinforcing phase compared to the gas-generated coating. In addition, two types of tungsten carbide, WC and W_2C, were identified in the PTA-generated surfacing. Complete elimination of dissolution cannot be possible, but its minimization would significantly improve material properties. The occurrence of secondary carbides was observed in both of the coatings. The formation of secondary carbides may also be related to the elements' heat treatment after surfacing to improve the base material, which should be further investigated. The microstructure of the surfacing affects its mechanical properties. In terms of usability, the PTA-generated surfacing was found to be better. It was characterized by a lower hardness of both the substrate and the overlay matrix, but a higher hardness of the reinforcing phase. The study showed that it exhibited higher impact strength and abrasion resistance than the surfacing produced by the gas method. Using the PTA method and modifying the material composition has brought many advantages, both in the process's automation and the obtained properties. Nevertheless, the observed imperfections, such as the lack of homogeneity of the reinforcing phase distribution, the partial dissolution of primary carbides, and the formation of brittle secondary carbides, leave room for even more significant improvement in the materials produced.

Acknowledgements

The work was carried out within the subvention 2019–2022 "Materials for work in extreme conditions" – Faculty of Materials Science and Engineering Warsaw University of Technology

References

[1] Franca LF. Drilling action of roller-cone bits: modeling and experimental validation. *J Energy Resour Technol*. 2010;132(4): 043101. doi:10.1115/1.4003168.

[2] Glinik Drilling Tools Catalog 2021. `https://glinik.com.pl/wp-content/uploads/2021/08/Catalog-2021_-v1_EN_compressed-2.pdf`. [Accessed 3rd April 2023].

[3] Šporin J, Mrvar P, Janc B, Vukelić Ž. Expression of the self-sharpening mechanism of a roller cone bit during wear due to the influence of the erosion protection carbide coating. *Coat.* 2021;11(11): 1308. doi:10.3390/coatings11111308.

[4] Sumrunpis N. Types of drilling bits. Weblog. `https://petgeo.weebly.com/types-of-drilling-bits.html` [Accessed 7th April 2023].

[5] Abbas RK. A review on the wear of oil drill bits (conventional and the state of the art approaches for wear reduction and quantification). *Eng Fail Anal*. 2018;90: 554–584. doi:10.1016/j.engfailanal.2018.03.026.

[6] Abbas RK, Ghanbarzadeh A, Hassanpour A. A novel method for estimating the real-time dullness of tricone oil drill bits. *Eng Fail Anal.* 2020;109:104386. doi:10.1016/j.engfailanal.2020.104386.

[7] Šporin J, Mrvar P, Petrič M, Vižintin G, Vukelić Ž. The characterization of wear in roller cone drill bit by rock material – sandstone. *J Pet Sci Eng.* 2019;173: 1355–1367. doi:10.1016/j.petrol.2018.10.090.

[8] Bu CG. Radial clearance is key factor affecting roller bearing life prediction in tricone bit. *Adv Mater Res.* 2008;44: 233–238. doi:10.4028/www.scientific.net/amr.44-46.233.

[9] Prakash S, Mukhopadhyay AK. Reliability analysis of tricone roller bits with tungsten carbide insert in blasthole drilling. *Int J Min Reclam Environ*. 2018;34(2): 101–118. doi:10.1080/17480930.2018.1530055.

[10] Larsen-Basse J. Wear of hard-metals in rock drilling: a survey of the literature. *Pow Metal.* 1973;16(31): 1–32. 10.1179/pom.1973.16.31.001.

[11] Šporin J, Balaško T, Mrvar P, Janc B, Vukelić Ž. Change

of the properties of steel material of the roller cone bit due to the influence of the drilling operational parameters and rock properties. *Energies.* 2020;13(22): 5949. doi:10.3390/en13225949.

[12] Xiao Q, Sun WL, Yang KX, Xing XF, Chen ZH, Zhou HN. Wear mechanisms and micro-evaluation on WC particles investigation of WC-FE composite coatings fabricated by laser cladding. *Surf Coat Technol*. 2021;420: 127341. doi:10.1016/j.surfcoat.2021.127341.

[13] Fang Z, Griffo A, White B, Belnap D, Hamilton R, Portwood G, Cox P, Hilmas G, Bitler J. Chipping resistant polycrystalline diamond and carbide composite materials for roller cone bits. In: SPE Annual Technical Conference and Exhibition. 2001. doi:10.2118/71394-MS.

[14] Ndlovu S, Durst K, Göken M. Investigation of the sliding contact properties of WC-Co hard metals using nanoscratch testing. *Wear.* 2007;263(7-12): 1602–1609. doi: 10.1016/j.wear.2006.11.044.

[15] Beste U, Jacobson S. A new view of the deterioration and wear of WC/Co cemented carbide rock drill buttons *Wear*. 2008;264(11-12): 1129–1141. doi:10.1016/j.wear.2007.01.030.

[16] Badisch E, Kirchgaßner M. Influence of welding parameters on microstructure and wear behaviour of a typical NICRBSI hardfacing alloy reinforced with tungsten carbide. *Surf Coat Technol*. 2008;202(24); 6016–6022. doi:10.1016/j.surfcoat.2008.06.185.

[17] Katiyar PK, Singh PK, Singh R, Kumar A. Modes of failure of cemented tungsten carbide tool bits (WC/CO): A study of wear parts. *Int J Refract Metals Hard Meterials.* 2016;54: 27–38. doi:10.1016/j.ijrmhm.2015.06.018.

[18] Liu W, Gao D. Microstructure and wear of Ni-WC Hardfacing used for steel-body PDC bits. *Int J Refract Metals Hard Meterials*. 2021;101: 105683. doi:10.1016/j.ijrmhm.2021.105683.

[19] Garcia-Ayala EM, Tarancon S, Gonzalez Z, Ferrari B, Pastor JY, Sanchez-Herencia AJ. Processing of WC/W composites for extreme environments by colloidal dispersion of powders and SPS sintering. *Int J Refract Metals Hard Meterials*. 2019;84: 105026. doi:10.1016/j.ijrmhm.2019.105026.

[20] Maroli B, Dizdar S. Effect of type and amount of tungsten carbides on the abrasive wear of laser cladded nickel based coatings. *ITSCE*. 2015: 11-14. doi:10.31399/asm.cp.itsc2015p0345.

[21] Czupryński A. Microstructure and abrasive wear resistance of metal matrix composite coatings deposited on steel grade AISI 4715 by Powder Plasma transferred arc welding part 2. Mechanical and structural properties of a nickel-based alloy surface layer reinforced with particles of tungsten carbide and synthetic metal–diamond composite, *Materials.* 2021;14(11): 2805. doi:10.3390/ma14112805.

[22] Huang Z, Li G. Failure analysis of roller cone bit bearing based on mechanics and microstructure. *J Fail Anal Prev*. 2018;18: 342–349. doi:10.1007/s11668-018-0419-3.

[23] Li Q, Lei TC, Chen WZ. Microstructural characterization of WCP reinforced Ni–Cr–B–Si–C composite coatings. *Surf Coat Technol*. 1999;114(2-3):285–291. doi:10.1016/s0257-8972(99)00056-0.

[24] Zhong M, Liu W, Yao K, Goussain JC, Mayer C, Becker A. Microstructural evolution in high power laser cladding of stellite 6+WC layers. *Surf CoatTechnol*. 2002; doi:10.1016/s0257-8972(02)00165-2.

[25] Zhong M, Liu W. Microstructure evolution of Stellite 6+WC by high power laser cladding. *Acta Metal Sin*. 202;38: 495–500. doi:10.1016/S0257-8972(02)00165-2.

[26] Liyanage T, Fisher G, Gerlich AP. Microstructures and abrasive wear performance of PTAW deposited ni–WC overlays using different Ni-alloy chemistries. *Wear.* 2012;274: 345–354. doi:10.1016/j.wear.2011.10.001.

[27] Gassmann RC. Laser cladding with (WC+W_2C)/co–CR–C and (WC+W_2C)/Ni–B–Si composites for enhanced abrasive wear resistance. *Mater Sci Technol.* 1996;12(8): 691–696. doi:10.1179/mst.1996.12.8.691.

[28] Sue A, Sreshta H, Qiu BH. Improved hardfacing for drill bits and drilling tools. *J Therm Spray Technol.* 2011;20: 372–377. doi:10.1007/s11666-010-9569-x.

[29] Marques PV, da Trevisan R. ARC fusion of self-fluxed nickel alloys. *J Braz Soc Mech Sci.* 2000;22: 379–387. doi:10.1590/s0100-73862000000300001.

[30] Grigorescu I. Phase characterization in ni alloy-hard carbide composites for fused coatings. *Surf Coat Technol.* 1995;76: 494–498. doi:10.1016/02578-9729(50)25111-.

[31] Hamar-Thibau S, Valignat N, Lebaili S. In Int. Congr. X-ray Optics and Microanalysis, Manchester, 1992, Inst. Phys. Conf. Ser. No. 130,2: 189–192.

[32] Yang L, Yu T, Li M, Zhao Y, Sun J. Microstructure and wear resistance of in-situ synthesized ti(c, N) ceramic reinforced Fe-based coating by laser cladding. *Ceram Int.* 2018;18: 22538–22548. doi:10.1016/j.ceramint.2018.09.025.

[33] Fernández MR, García A, Cuetos JM, González R, Noriega A, Cadenas M. Effect of actual WC content on the reciprocating wear of a laser cladding NiCrBSi alloy reinforced with WC. *Wear*. 2015l;324, 80–89. doi:10.1016/j.wear.2014.12.021.

[34] Tehrani HM, Shoja-Razavi R, Erfanmanesh M, Hashemi SH, Barakat M. Evaluation of the mechanical properties of WC-Ni composite coating on an AISI 321 steel substrate. *Opt Laser Technol.* 2020;127: 106138. doi:10.1016/j.optlastec.2020.106138.

Received 2023-04-13
Accepted 2023-05-29